nature energy

SUPPLEMENTARY INFORMATION

https://doi.org/10.1038/s41560-018-0184-2

In the format provided by the authors and unedited.

Nucleation of dislocations and their dynamics in layered oxide cathode materials during battery charging

A. Singer[1,7], M. Zhang[2], S. Hy[2], D. Cela[1], C. Fang[2], T. A. Wynn[2], B. Qiu[3], Y. Xia[3], Z. Liu[3], A. Ulvestad[4], N. Hua[1], J. Wingert[1], H. Liu[2], M. Sprung[5], A. V. Zozulya[5,8], E. Maxey[6], R. Harder[6], Y. S. Meng[2]* and O. G. Shpyrko[1]*

[1]Department of Physics, University of California-San Diego, La Jolla, California, USA. [2]Department of NanoEngineering, University of California-San Diego, La Jolla, California, USA. [3]Ningbo Institute of Materials Technology and Engineering (NIMTE), Chinese Academy of Sciences, Zhejiang, China. [4]Materials Science Division, Argonne National Laboratory, Argonne, Illinois, USA. [5]Deutsches Elektronen-Synchrotron DESY, Hamburg, Germany. [6]X-ray Science Division, Advanced Photon Source, Argonne, Illinois, USA. [7]Present address: Cornell University, Ithaca, New York, USA. [8]Present address: European XFEL GmbH, Schenefeld, Germany. *e-mail: shirleymeng@ucsd.edu; oshpyrko@physics.ucsd.edu

Supplementary Figures

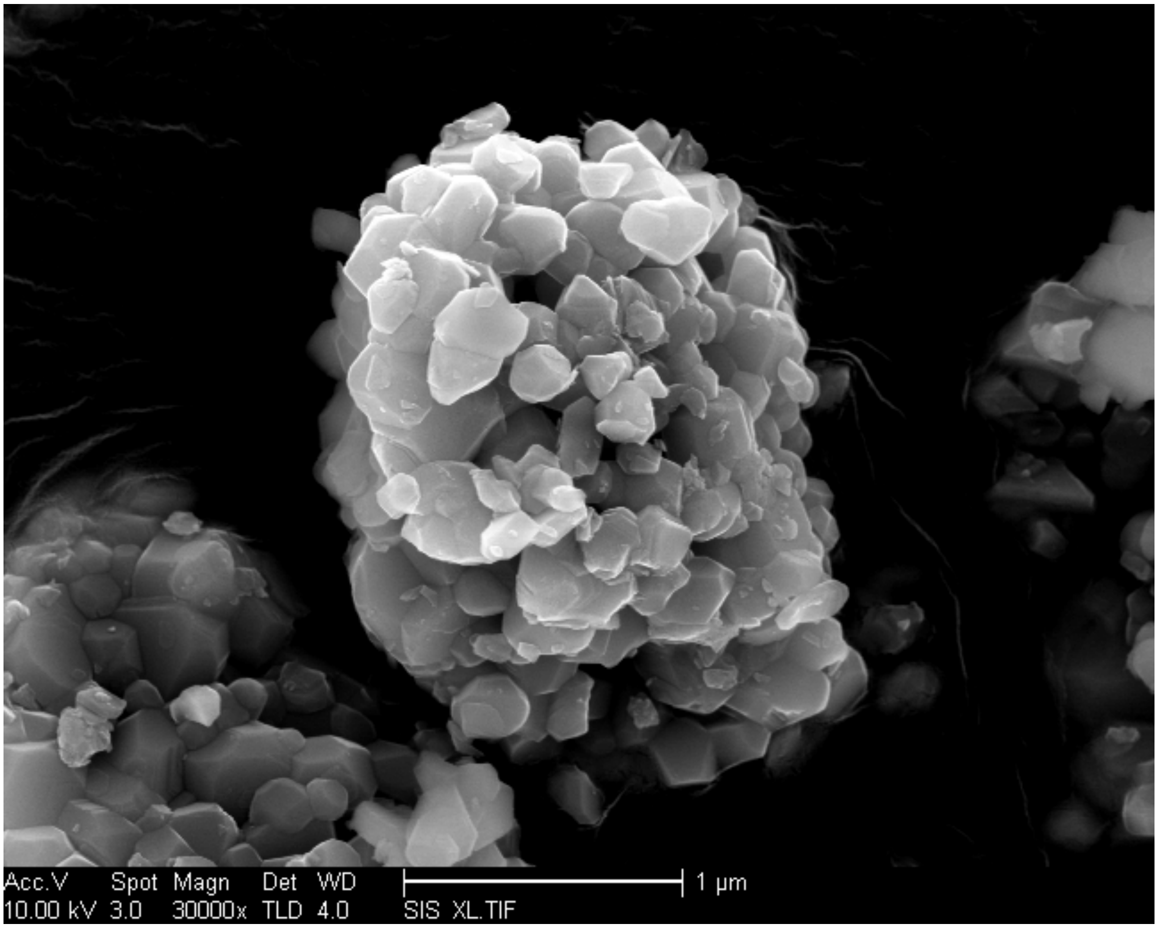

Supplementary Figure 1: Scanning electron microscopy image of the pristine LRLO material. The primary particles (sub-micron single crystallites) are agglomerated to larger secondary particles to improve the volumetric energy density.

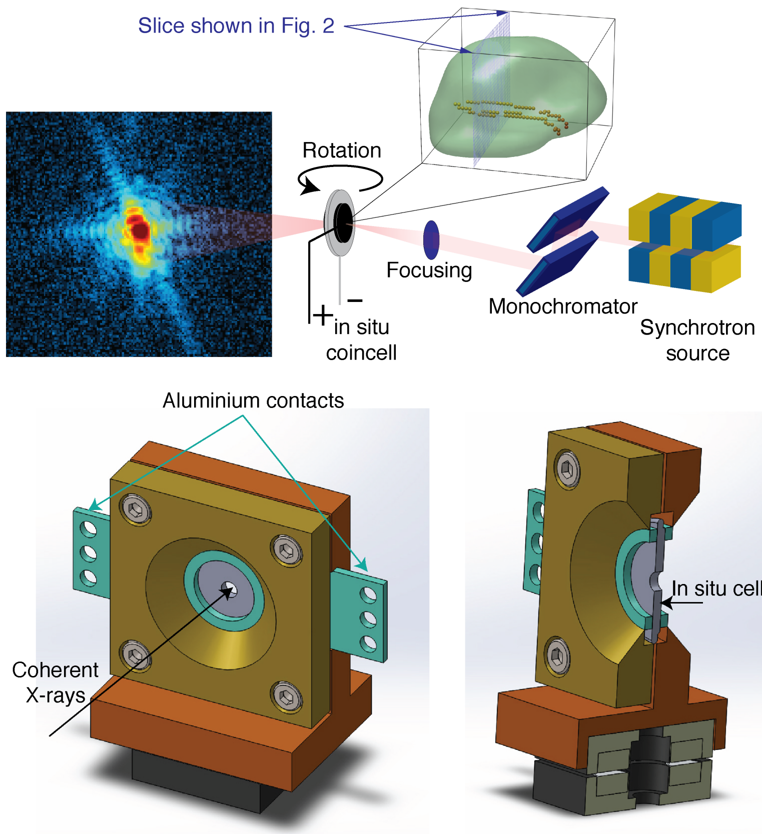

Supplementary Figure 2: Experimental description. Schematic of the experimental arrangement (top, the slice through the 3D volume of the particle shown in Fig. 2 is indicated) and the sample holder with the *in situ* coin cell used in both experiments (bottom).

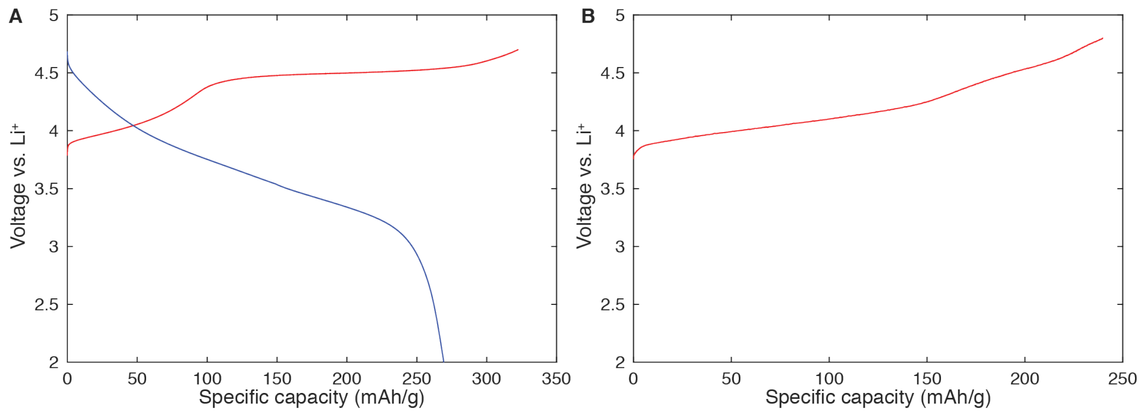

Supplementary Figure 3: Electrochemical performance. a Specific capacity of the *in situ* LRLO cell measured simultaneously with the x-ray imaging data shown in Figs. 2 and S7. **b** Specific capacity of the *in situ* NCA cell measured simultaneously with the x-ray imaging data shown in Fig. 3.

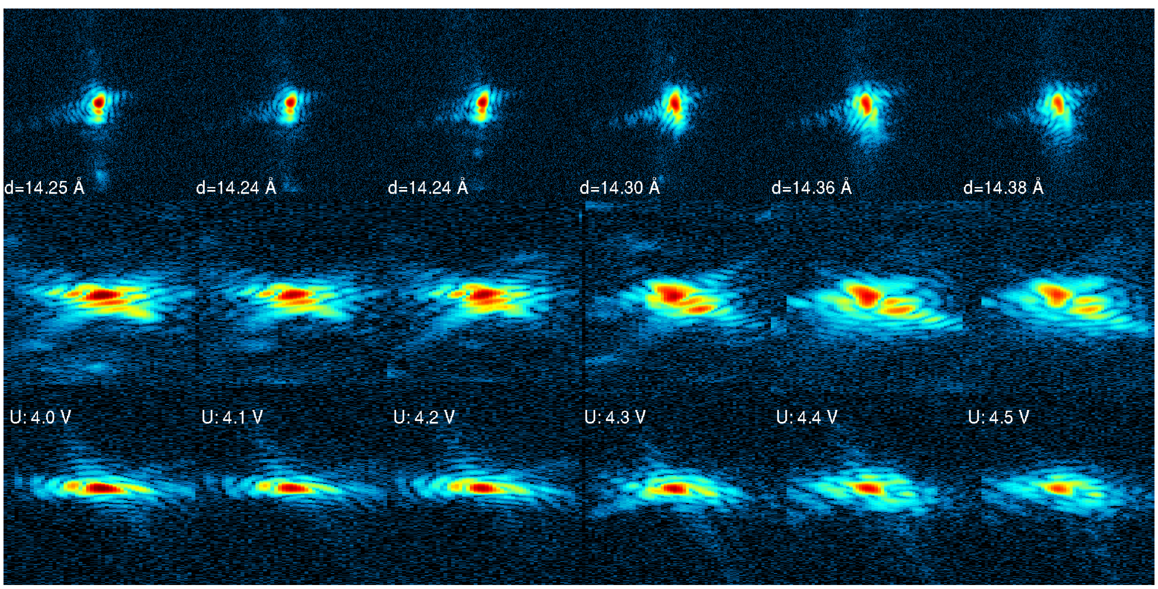

Supplementary Figure 4: Diffraction data collected for the particle shown in Fig. 1 and 2 of the main text. The voltage and the average lattice parameter are indicated. The average lattice parameter was determined from the center of mass of the 3D reciprocal space data around the Bragg peak. The top row shows images as seen on the detector during the measurement, the whole pattern is 0.027 $Å^{-1}$ X 0.027 $Å^{-1}$ in size. The second row and third rows show two different orthogonal views of the 3D diffraction pattern collected during the rocking series. The scattering vector is approximately vertical (top), out of plane (middle), horizontal (bottom).

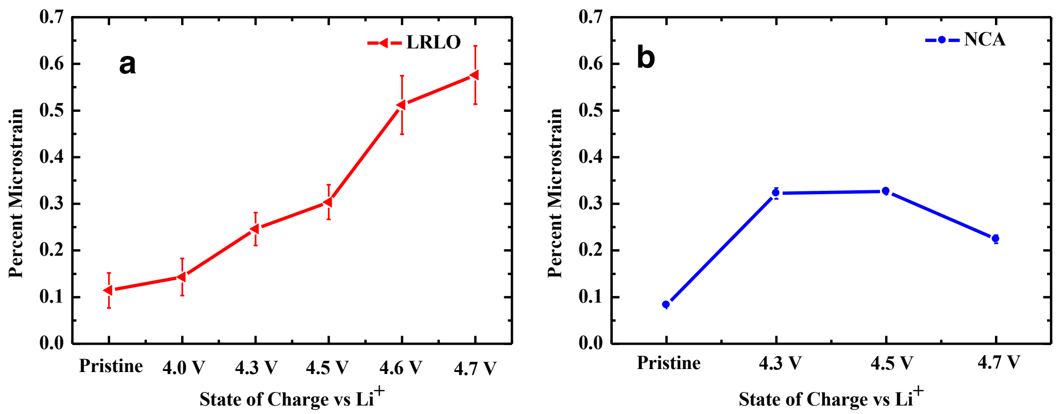

Supplementary Figure 5: Comparison of microstrain changes for different states of charge of LRLO and NCA samples determined from the Williamson-Hall analysis of the Bragg peak widths from conventional x-ray diffraction experiments on a large number of particles. The data for LRLO (a) was measured *in situ*, while NCA (b) was measured *ex situ*.

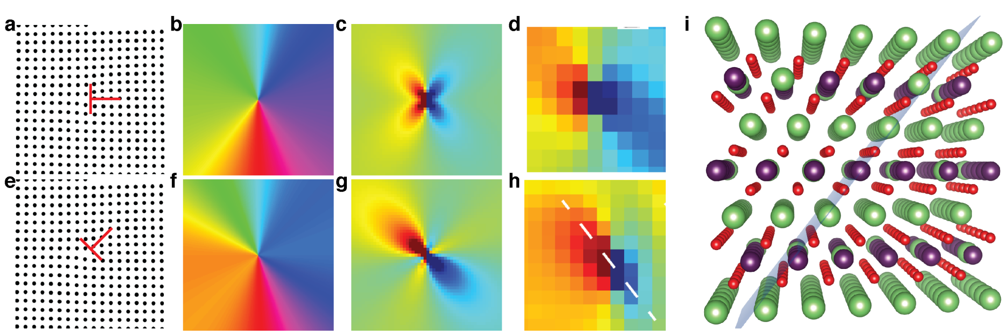

Supplementary Figure 6: Microscopic model of the displacement field and strain around a dislocation. a Schematic of an edge dislocation with extra half plane parallel to the layers and the corresponding displacement field **b** and strain field **c**. **d** Strain field around a dislocation in NCA from Fig. 3 (4.2 V). **e** A schematic of an edge dislocation with the extra half plane building an angle with the layers and the corresponding displacement field **f** and strain **g**. **h** Strain field around a dislocation in LRLO from Fig. 2 (4.3 V). **i** The geometry of the possible orientation of the extra half plane {403} in LRLO is indicated by semitransparent blue plane through the center of the image.

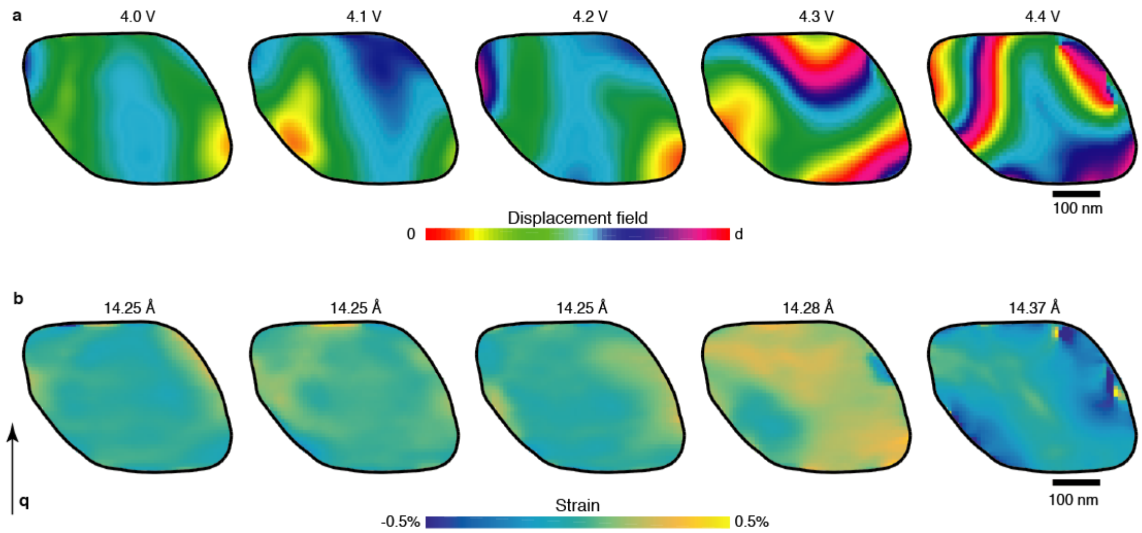

Supplementary Figure 7: *In-situ* evolution of a second LRLO nanoparticle during charge. a The changes in the displacement field along the (001) direction in a plane through the nanoparticle during charge. The voltage vs. Li^+ is indicated at the top. Edge dislocations emerge at 4.4 V vs. Li^+. A screw dislocation is present in this nanoparticle in the pristine state and through the charge. **b** The strain along the (001) direction inside of the nanoparticle calculated from the 3D displacement fields in **a**. The strain is shown around the average lattice constant indicated at the top.

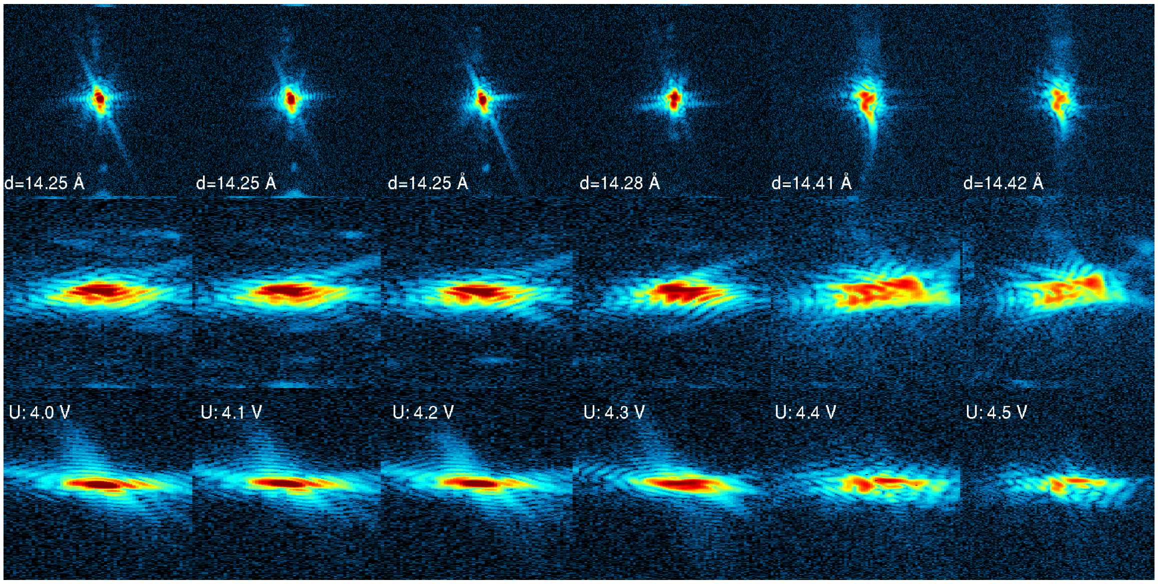

Supplementary Figure 8: Diffraction data collected for the particle whose microstrain is shown in Fig. 4 in the main text by magenta symbols. The reconstructions are shown in Fig. S7. The voltage and the average lattice parameter determined from the center of the diffraction peak are indicated. The top row shows images as seen on the detector during the measurement, the whole pattern is 0.027 $Å^{-1}$ X 0.027 $Å^{-1}$ in size. The second row and third rows show two different orthogonal views of the 3D diffraction pattern collected during the rocking series. The scattering vector is approximately vertical (top), out of plane (middle), horizontal (bottom).

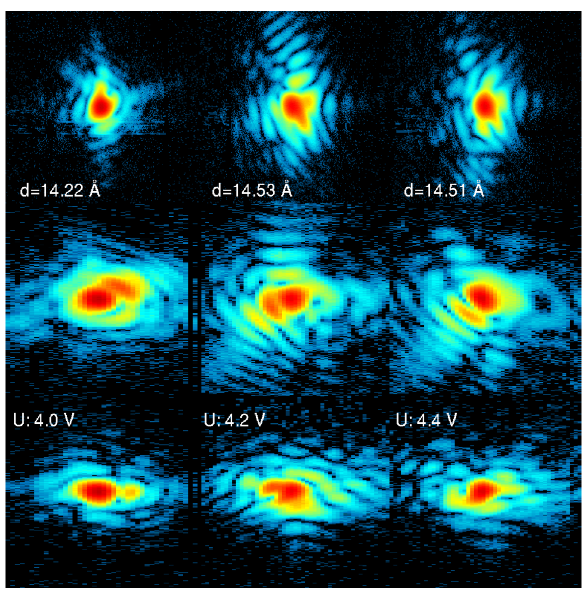

Supplementary Figure 9: Diffraction data collected for the NCA particle shown in Fig. 3 in the main text. The top row shows images as seen on the detector, the whole pattern is 0.038 $Å^{-1}$ X 0.038 $Å^{-1}$ in size. The second row and third rows show two different orthogonal views of the 3D diffraction pattern collected during the rocking series. The scattering vector is approximately vertical (top), out of plane (middle), horizontal (bottom).

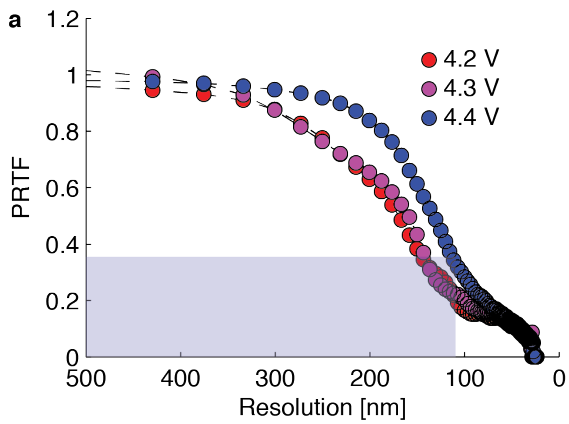

Supplementary Figure 10: Phase retrieval transfer function (PRTF). a PRTF for the reconstructions shown in Fig. 2 of the main text. **b** PRTF for the particle shown in Fig. S7.

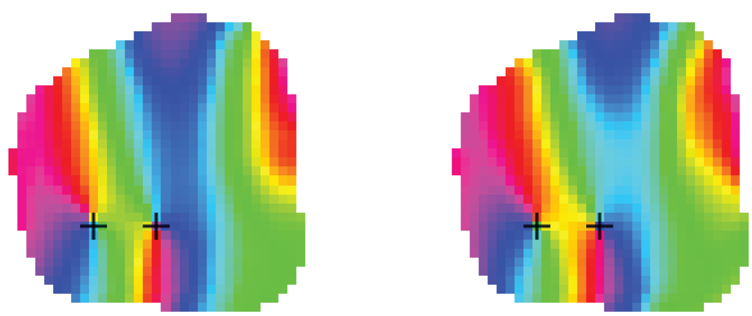

Supplementary Figure 11: Comparison between two different reconstructions of the same rocking scan. Note that although the results from reconstruction procedures initiated from different random starts differ slightly, which is reflected in the PRTF resolution of about 100 nm, the positions of the dislocations are consistent between different reconstructions to a much better resolution (within a pixel, i.e. 7.75 nm).

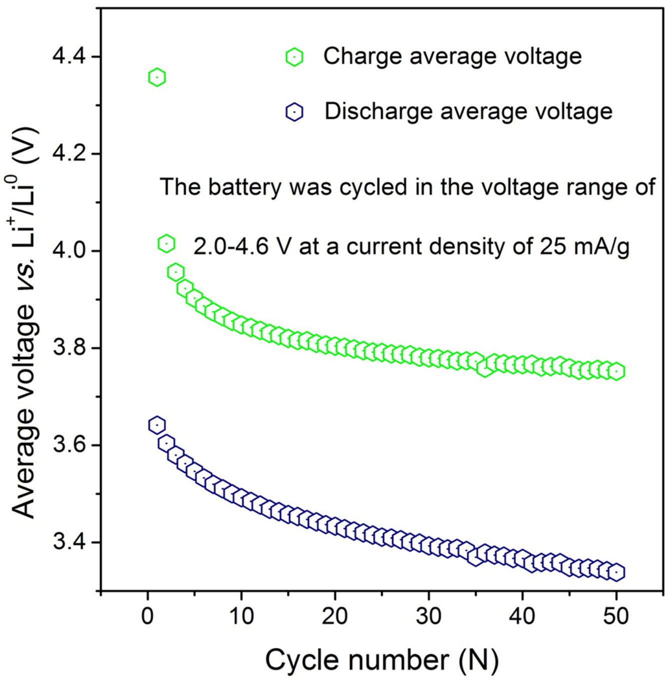

Supplementary Figure 12: The average charge and discharge voltage of LRLO cathode with Li-metal as anode for the first 50 cycles.

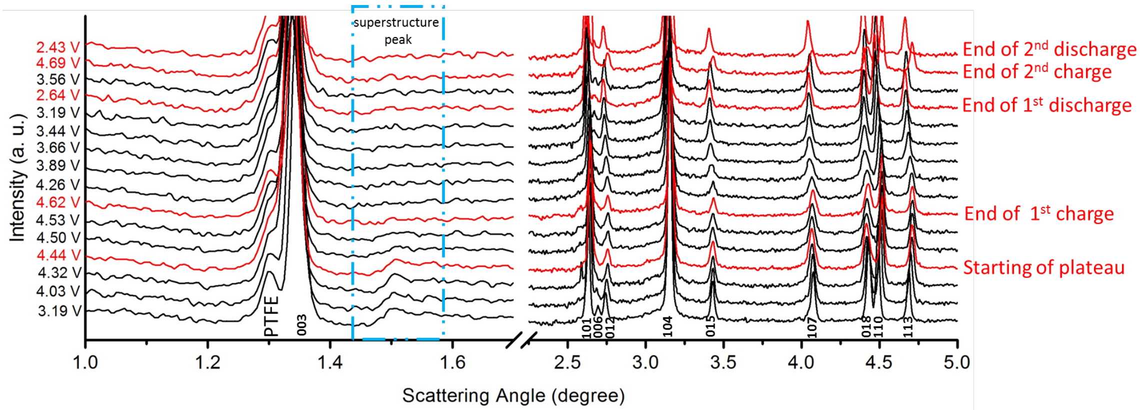

Supplementary Figure 13: The evolution of the superstructure peak intensity during the subsequent cycling. The data for LRLO was measured *in situ* at the Advanced Photon Source at Argonne National Laboratory. The wavelength of the x-ray source was 0.11165 Å. Figure 4c shows the diffraction intensity integrated over the region indicated by the blue box.

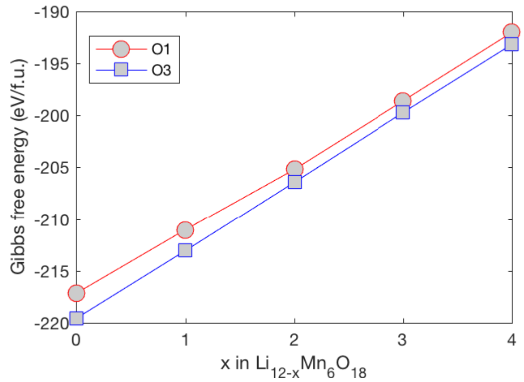

Supplementary Figure 14: The Gibbs free energy for each delithiation composition of the supercell with O3 and O1 stacking. The energy difference reduces for lower lithium concentrations as described in the main text.

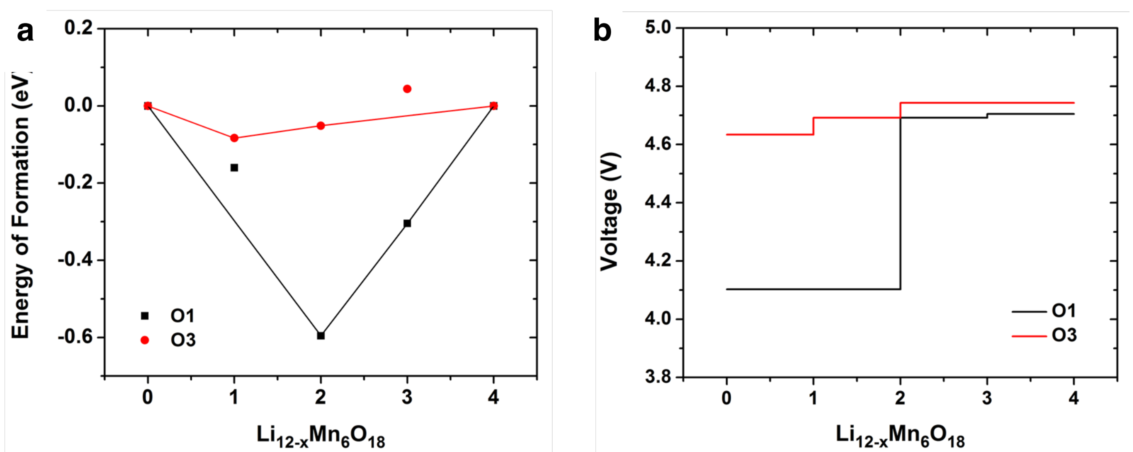

Supplementary Figure 15: Results of the first principle calculations. a The formation energy and **b** calculated voltage of $Li_{12-x}Mn_6O_{18}$ ($0 \leqslant x \leqslant 4$) for stacking sequence O3 and O1.

Normalized Li Concentr.	Gibbs free energy (eV/f.u.)	
	O1	O3
12	-217.2	-219.6
11	-211.1	-213.1
10	-205.2	-206.4
9	-198.6	-199.7
8	-192.0	-193.1

Supplementary Table 1: The Gibbs free energy for each delithiation composition of the supercell with O3 and O1 stacking.